Cell Reports, Volume *42*

Supplemental information

Limiting Mrs2-dependent mitochondrial Mg^{2+} uptake induces metabolic programming in prolonged dietary stress

Travis R. Madaris, Manigandan Venkatesan, Soumya Maity, Miriam C. Stein, Neelanjan Vishnu, Mridula K. Venkateswaran, James G. Davis, Karthik Ramachandran, Sukanthathulse Uthayabalan, Cristel Allen, Ayodeji Osidele, Kristen Stanley, Nicholas P. Bigham, Terry M. Bakewell, Melanie Narkunan, Amy Le, Varsha Karanam, Kang Li, Aum Mhapankar, Luke Norton, Jean Ross, M. Imran Aslam, W. Brian Reeves, Brij B. Singh, Jeffrey Caplan, Justin J. Wilson, Peter B. Stathopulos, Joseph A. Baur, and Muniswamy Madesh

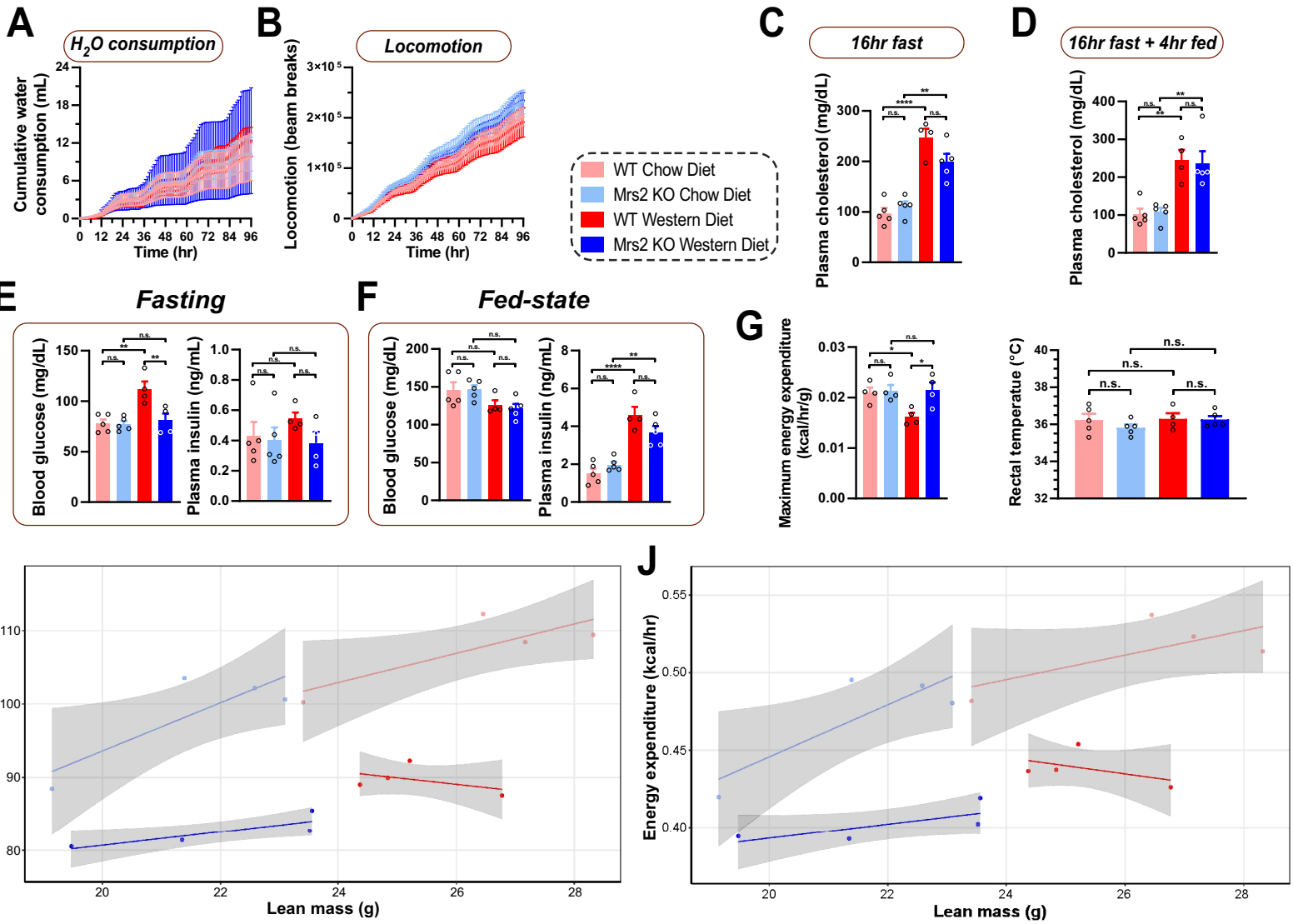
A
H_2O consumption
Cumulative water consumption (mL)
Time (hr)
B
Locomotion
Locomotion (beam breaks)
Time (hr)
WT Chow Diet
Mrs2 KO Chow Diet
WT Western Diet
Mrs2 KO Western Diet
C
16hr fast
Plasma cholesterol (mg/dL)
D
16hr fast + 4hr fed
Plasma cholesterol (mg/dL)
E
Fasting
Blood glucose (mg/dL)
Plasma insulin (ng/mL)
F
Fed-state
Blood glucose (mg/dL)
Plasma insulin (ng/mL)
G
Maximum energy expenditure (kcal/hr/g)
Rectal temperatue (°C)
I
Oxygen consumption (mL/hr)
Lean mass (g)
J
Energy expenditure (kcal/hr)
Lean mass (g)

Figure S1: Assessment of Water Consumption, Locomotion, And Plasma Cholesterol in WT And *Mrs2*$^{-/-}$ Mice (Related to Figure 1).

A and B) Water consumption and locomotion of mice during metabolic screening with Promethion system.
C and D) Plasma levels of cholesterol after mice were subjected to 16 hrs fasting (C) followed by 4 hrs of fed state (D). WT and *Mrs2*$^{-/-}$ mice fed either a WD or CD for one year. n=4-5 mice per group.
E and F) Blood glucose and plasma insulin levels in fasting (left) or fed (right) states of CD or WD-fed (1 year) WT or *Mrs2*$^{-/-}$ mice.
G) Maximum energy expenditure calculated from Fig. 1G from mice from the four groups. n=4 mice per group.
H) Average rectal temperature from mice from the four groups before indirect calorimetry. n=4-5 mice per group.
I and J) ANCOVA plots of indirect calorimetry data of oxygen consumption (G) and energy expenditure (H) with lean mass as a covariate. n=4 mice per group.
A-H) Data is mean ± SEM; ****= $P<0.0001$, **= $P<0.01$, *= $P<0.05$, n.s.=not significant.

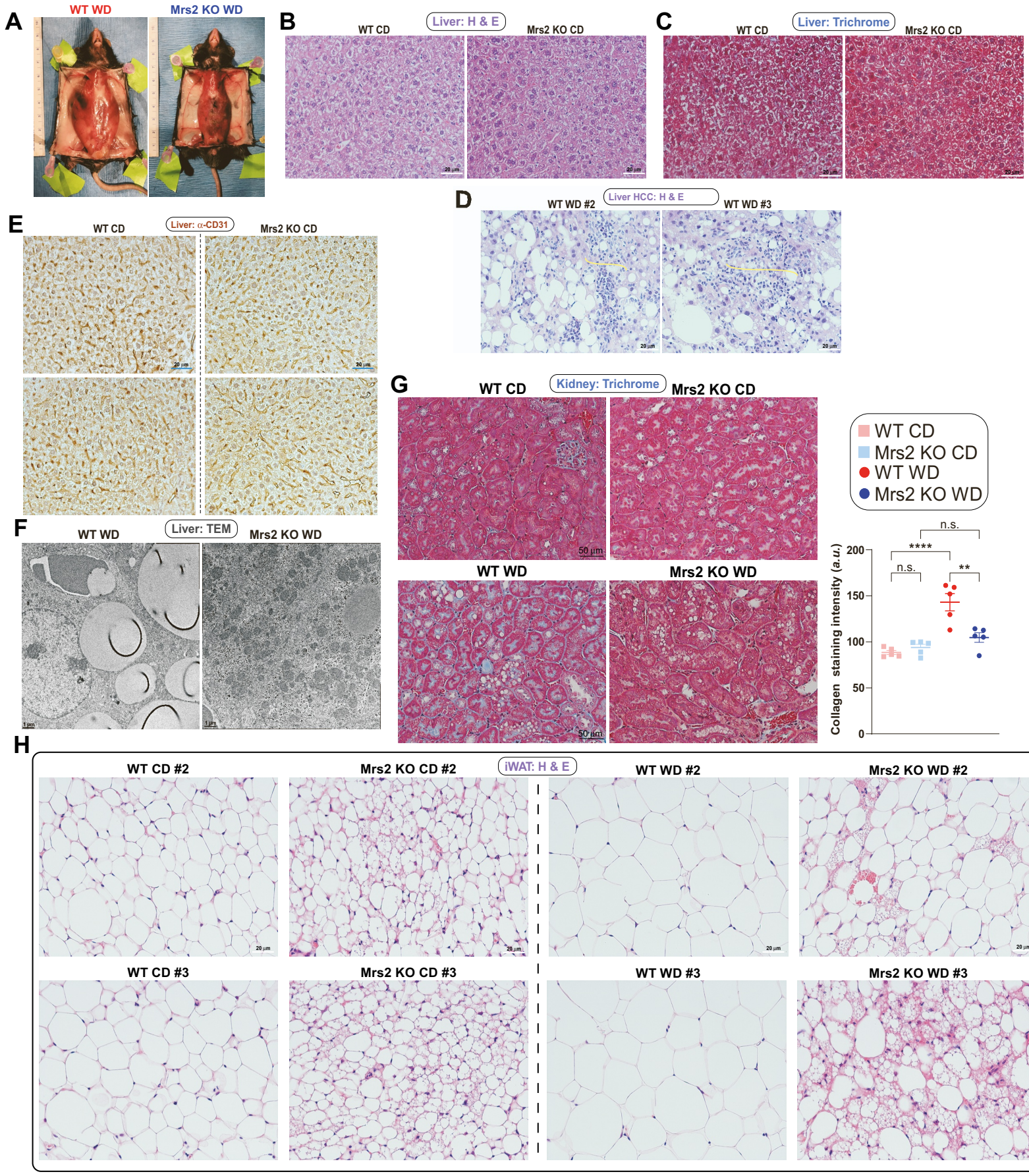
A
WT WD
Mrs2 KO WD
B
Liver: H & E
WT CD
Mrs2 KO CD
C
Liver: Trichrome
WT CD
Mrs2 KO CD
D
Liver HCC: H & E
WT WD #2
WT WD #3
E
Liver: α-CD31
WT CD
Mrs2 KO CD
F
Liver: TEM
WT WD
Mrs2 KO WD
G
Kidney: Trichrome
WT CD
Mrs2 KO CD
WT WD
Mrs2 KO WD
50 μm
WT CD
Mrs2 KO CD
WT WD
Mrs2 KO WD
n.s.
****
n.s.
**
Collagen staining intensity (a.u.)
200
150
100
50
0
H
iWAT: H & E
WT CD #2
Mrs2 KO CD #2
WT WD #2
Mrs2 KO WD #2
WT CD #3
Mrs2 KO CD #3
WT WD #3
Mrs2 KO WD #3

Figure S2: Microscopic Assessment of Fibrosis, Microvascular Density, and Ultrastructure in WT and *Mrs2*$^{-/-}$ Mice (Related to Figure 2).

A) Gross anatomy of Western diet-fed mice after 1 year on diet. Wildtype (left) and *Mrs2*$^{-/-}$ (right).
B and C) Representative liver tissue sections stained with hematoxylin & eosin (H&E) (B) and Masson's trichrome (C) from WT and *Mrs2*$^{-/-}$ chow diet (CD) fed after 1 year diet period. n= 3 mice per group.
D) Representative images of H&E-stained liver sections from 1-year WD fed mice. Note foci of immune cell infiltration as an indicator of tumor nodules appearing in the liver (yellow curve).
E) Immunohistochemical analysis of vascular density (α-CD31) in liver samples obtained from CD-fed WT (left) and *Mrs2*$^{-/-}$ mice after 1 year diet period. n=3 mice per group.
F) Representative transmission electron microscopy (TEM) images of liver sections from 1-year WD fed WT or *Mrs2*$^{-/-}$ mice. n= 3 mice per group.
G) Representative kidney sections stained with Masson's Trichrome from CD or WD-fed WT and *Mrs2*$^{-/-}$ after 1 year diet period. n=3 mice per group. Dot plot indicates the quantification of collagen staining. Randomly five slides were used for quantification. Mean ± SEM. **= P<0.01 ****= P<0.0001, n.s.= not significant.
H) Representative H&E-stained adipose tissue sections from remaining WT and *Mrs2*$^{-/-}$ chow diet (CD) or Western diet (WD) fed after 1 year diet period. Total n=3 mice per group.

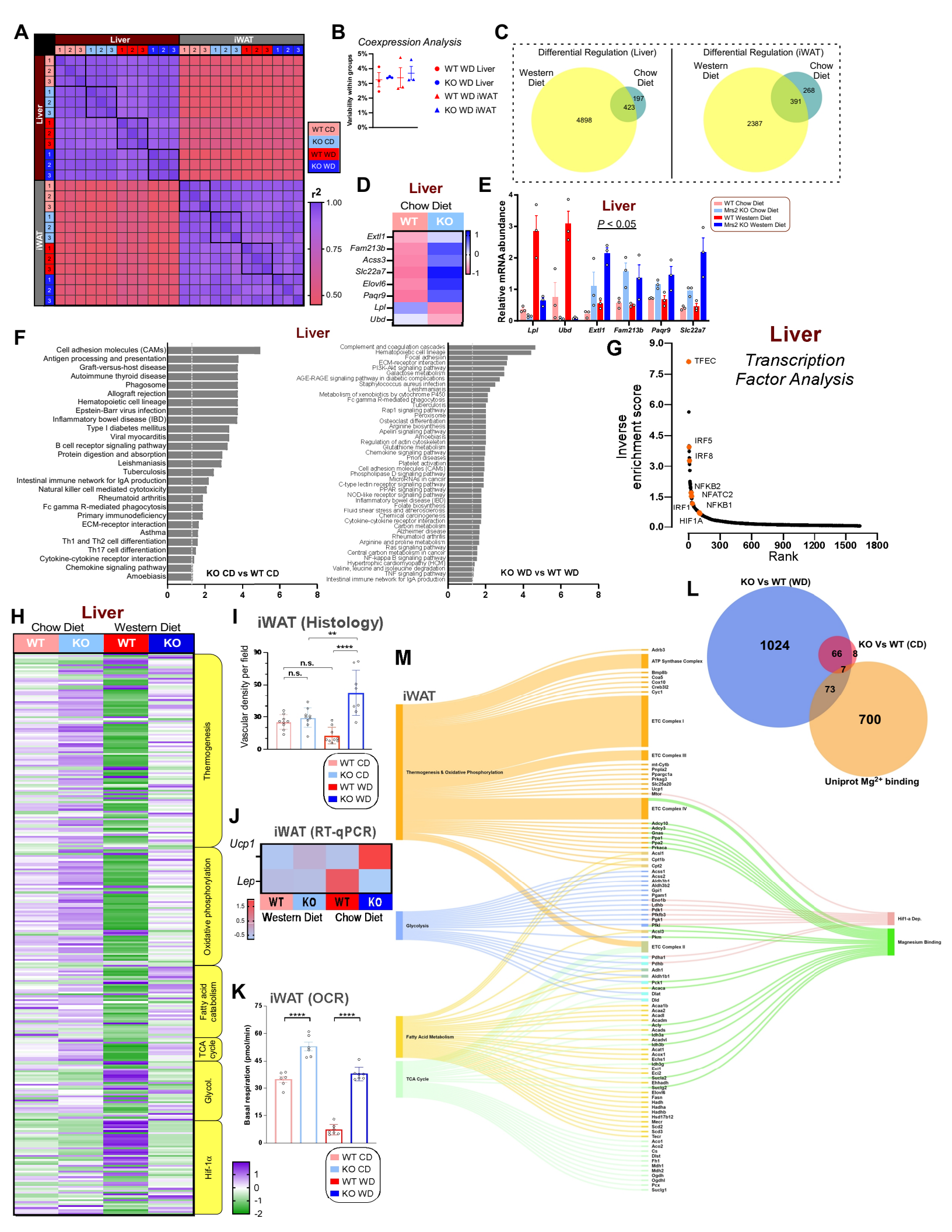
A
Liver
iWAT
WT CD
KO CD
WT WD
KO WD
r2
1.00
0.75
0.50
B
Coexpression Analysis
Variability within groups
WT WD Liver
KO WD Liver
WT WD iWAT
KO WD iWAT
C
Differential Regulation (Liver)
Western Diet
Chow Diet
4898
197
423
Differential Regulation (iWAT)
Western Diet
Chow Diet
2387
268
391
D
Liver
Chow Diet
WT
KO
Extl1
Fam213b
Acss3
Slc22a7
Elovl6
Paqr9
Lpl
Ubd
E
Liver
P < 0.05
Relative mRNA abundance
WT Chow Diet
Mrs2 KO Chow Diet
WT Western Diet
Mrs2 KO Western Diet
Lpl
Ubd
Extl1
Fam213b
Paqr9
Slc22a7
F
Liver
Cell adhesion molecules (CAMs)
Antigen processing and presentation
Graft-versus-host disease
Autoimmune thyroid disease
Phagosome
Allograft rejection
Hematopoietic cell lineage
Epstein-Barr virus infection
Inflammatory bowel disease (IBD)
Type I diabetes mellitus
Viral myocarditis
B cell receptor signaling pathway
Protein digestion and absorption
Leishmaniasis
Tuberculosis
Intestinal immune network for IgA production
Natural killer cell mediated cytotoxicity
Rheumatoid arthritis
Fc gamma R-mediated phagocytosis
Primary immunodeficiency
ECM-receptor interaction
Asthma
Th1 and Th2 cell differentiation
Th17 cell differentiation
Cytokine-cytokine receptor interaction
Chemokine signaling pathway
Amoebiasis
KO CD vs WT CD
Complement and coagulation cascades
Hematopoietic cell lineage
Focal adhesion
ECM-receptor interaction
PI3K-Akt signaling pathway
Galactose metabolism
AGE-RAGE signaling pathway in diabetic complications
Staphylococcus aureus infection
Leishmaniasis
Metabolism of xenobiotics by cytochrome P450
Fc gamma R-mediated phagocytosis
Tuberculosis
Rap1 signaling pathway
Peroxisome
Osteoclast differentiation
Arginine biosynthesis
Apelin signaling pathway
Amoebiasis
Regulation of actin cytoskeleton
Glutathione metabolism
Chemokine signaling pathway
Prion diseases
Platelet activation
Cell adhesion molecules (CAMs)
Phospholipase D signaling pathway
MicroRNAs in cancer
C-type lectin receptor signaling pathway
PPAR signaling pathway
NOD-like receptor signaling pathway
Inflammatory bowel disease (IBD)
Folate biosynthesis
Fluid shear stress and atherosclerosis
Chemical carcinogenesis
Cytokine-cytokine receptor interaction
Carbon metabolism
Alzheimer disease
Rheumatoid arthritis
Arginine and proline metabolism
Ras signaling pathway
Central carbon metabolism in cancer
NF-kappa B signaling pathway
Hypertrophic cardiomyopathy (HCM)
Valine, leucine and isoleucine degradation
TNF signaling pathway
Intestinal immune network for IgA production
KO WD vs WT WD
G
Liver
Transcription Factor Analysis
TFEC
Inverse enrichment score
IRF5
IRF8
NFKB2
NFATC2
NFKB1
IRF1
HIF1A
Rank
H
Liver
Chow Diet
Western Diet
WT
KO
WT
KO
Thermogenesis
Oxidative phosphorylation
Fatty acid catabolism
TCA cycle
Glycol.
Hif-1α
I
iWAT (Histology)
Vascular density per field
n.s.
n.s.
**
****
WT CD
KO CD
WT WD
KO WD
J
iWAT (RT-qPCR)
Ucp1
Lep
WT
KO
WT
KO
Western Diet
Chow Diet
K
iWAT (OCR)
Basal respiration (pmol/min)
****
****
WT CD
KO CD
WT WD
KO WD
L
KO Vs WT (WD)
1024
KO Vs WT (CD)
66
8
7
73
700
Uniprot Mg2+ binding
M
iWAT
Thermogenesis & Oxidative Phosphorylation
Glycolysis
Fatty Acid Metabolism
TCA Cycle
ATP Synthase Complex
ETC Complex I
ETC Complex III
ETC Complex IV
ETC Complex II
Hif1-a Dep.
Magnesium Binding

Figure S3: RNA-seq Quality Control and Comparative Analyses of Differentially Regulated Gene Transcripts (Related to Figure 3).

A) Correlation (Pearson's r^2) heatmap of RNA-seq data.
B) Coexpression analysis of Western-diet fed groups to examine the variability between biological replicates (within group). %variability indicates the proportion of protein-coding genes that are uniquely expressed in a single replicate within the indicated group. Mean ± SEM.
C) Venn diagram depicts the differentially expressed protein-coding genes between WT and *Mrs2*$^{-/-}$ mice fed Western diet or chow diet (1 year diet period). Liver tissue (left) and iWAT (right).
D) Significant (adj. *P*<0.05) differentially expressed genes between *Mrs2*$^{-/-}$ CD and WT CD liver tissue shown as a heatmap. Values shown as row *z*-scores. n=3 mice/group.
E) Bar graph shows the differentially expressed genes (adj. *P*<0.05) shared in both CD comparison and WD comparison from *Mrs2*$^{-/-}$ and WT liver tissue. The corrected enrichment counts (FPKM) were normalized and expressed as relative mRNA abundance. n=3 mice per group.
F) Liver tissue KEGG gene set enrichment analysis with significantly differentially regulated pathways indicated (adjusted *P*<0.05). CD-fed mice (left) and WD-fed mice (right). The dotted line indicates the significance threshold.
G) Transcription factor enrichment analysis of liver tissue using utilizing ChEA ranking tool. Select transcription factors are highlighted. The y-axis is the mathematical inverse of the enrichment score x100. Based on differential expression analysis of Western-diet fed mice.
H) Targeted KEGG analysis of liver tissue from WT and *Mrs2*$^{-/-}$ mice fed CD or WD. The heatmap depicts all gene hits in selected KEGG pathways (see methods). Values shown as row *z*-scores. n=3 mice/group.
I) Microvascular densities in the adipose tissue were quantified from the H&E-stained tissues. Data expressed as the number of vasculatures/field n=3 mice per group. Nine images were chosen for the quantification. Mean ± SEM. ****= *P*<0.0001, **= *P*<0.01, n.s.= not significant.
J) Heatmap depicting relative fold-change (*Act* normalized) of *Ucp1* and *Lep* in iWAT (RT-qPCR) from WT and *Mrs2*$^{-/-}$ mice fed either CD or WD. n=4 mice per group.
K) Quantification of the basal OCR in fresh iWAT explant homogenate. Mean ± SEM. Two-tailed Student's *t*-test; ****=*p*<0.001.
L) Venn-diagram depicts the differential expression of Mg^{2+} binding protein transcripts. These candidate genes were extracted from Uniprot and compared between iWAT CD vs WD conditions of WT and *Mrs2*$^{-/-}$ mice.

M) Sankey plot diagram depicting the expression of differentially regulated genes between WT WD and *Mrs2*$^{-/-}$ WD animals (generated using SankeyMATIC). This diagram links the essential pathways that are modulated by $_{i}Mg^{2+}$and Hif1-α dependent signaling.

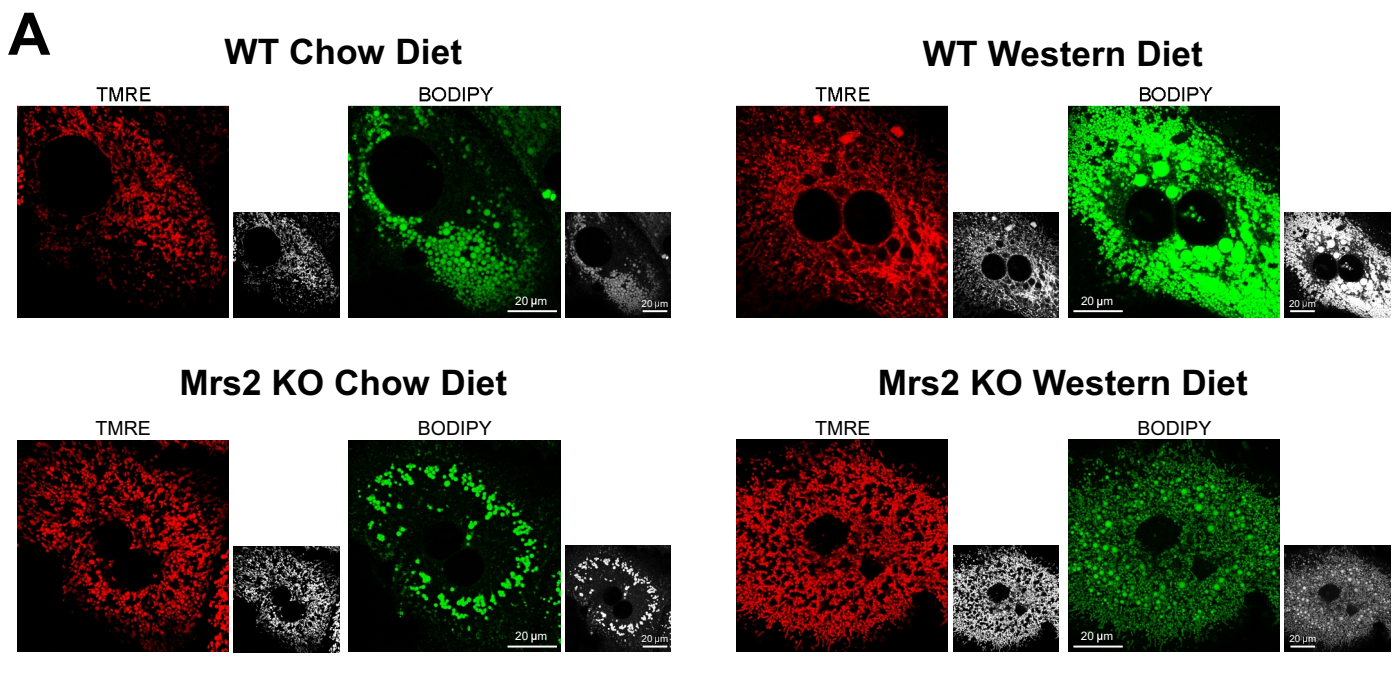
A
WT Chow Diet
TMRE
BODIPY
WT Western Diet
TMRE
BODIPY
Mrs2 KO Chow Diet
TMRE
BODIPY
Mrs2 KO Western Diet
TMRE
BODIPY
20 µm

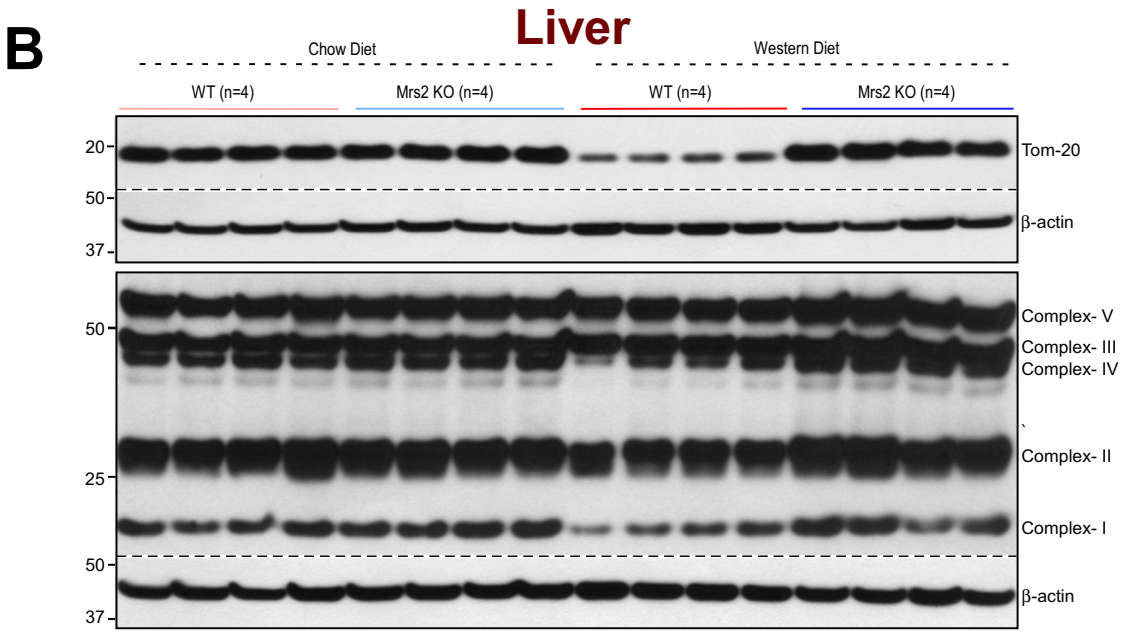
B
Liver
Chow Diet
Western Diet
WT (n=4)
Mrs2 KO (n=4)
WT (n=4)
Mrs2 KO (n=4)
20
50
37
Tom-20
β-actin
50
25
50
37
Complex- V
Complex- III
Complex- IV
Complex- II
Complex- I
β-actin

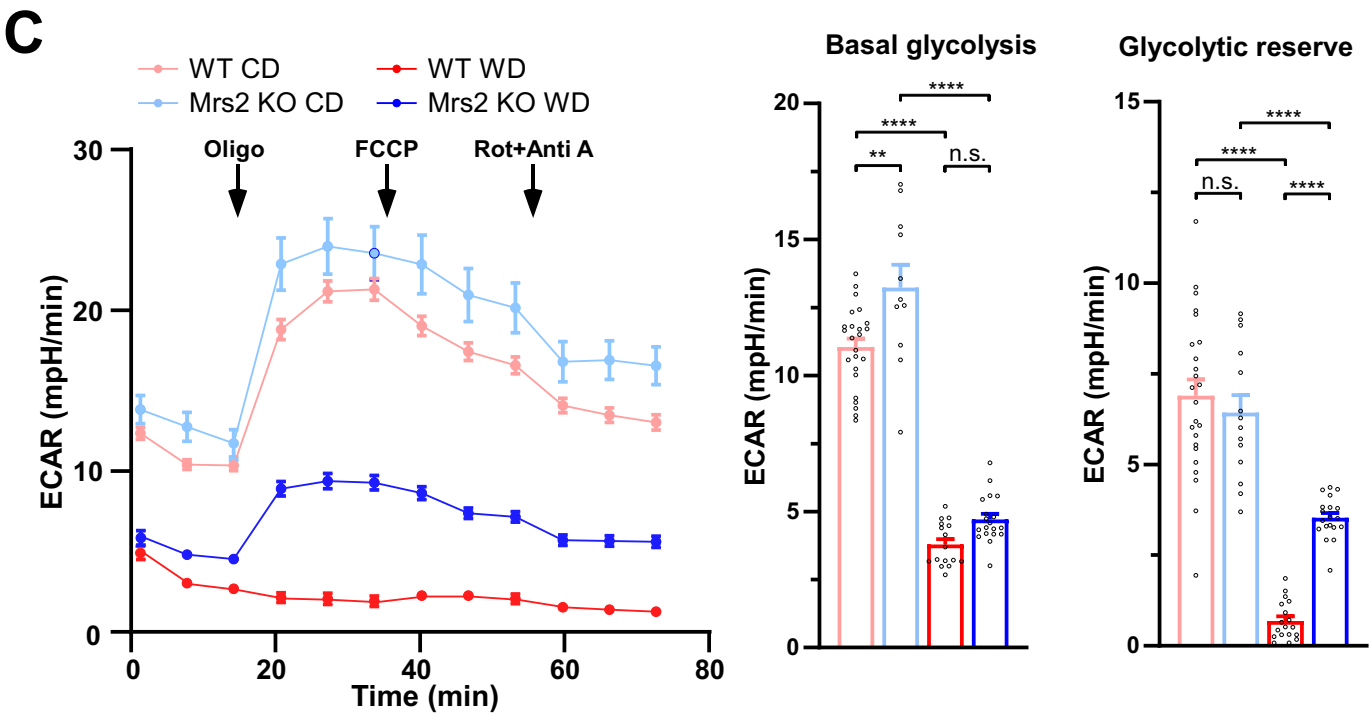
C
WT CD
WT WD
Mrs2 KO CD
Mrs2 KO WD
Oligo
FCCP
Rot+Anti A
ECAR (mpH/min)
Time (min)
Basal glycolysis
Glycolytic reserve
****
**
n.s.

Figure S4: Assessment of Hepatocyte Mitochondrial OXPHOS Complex Protein Abundance and Extracellular Acidification (Related to Figure 4).

A) Split channel confocal images from Fig. 4A. Hepatocytes stained with $\Delta\Psi_m$ indicator, TMRE (red, left images), lipid/fatty acid marker, BODIPY-488 (green, right images). Black and White images were generated for both TMRE and BODIPY staining (inset). 100x objective, scale bar 20 μm. n= 3 isolations per group.
B) Western blot depicting the abundance of mitochondrial OXPHOS complex protein in WT and *Mrs2*$^{-/-}$ liver from chow or western diet-fed mice. n=4 mice per group.
C) Traces (left) represent extracellular acidification rate (ECAR) in WT or *Mrs2*$^{-/-}$ hepatocytes isolated from CD or WD-fed mice (1 year diet period). Inhibitors (oligomycin, FCCP, and rotenone+antimycin added at the indicated time points. Bar charts show basal glycolysis and glycolytic reserve. Mean ± SEM. n=3-6. ****= $P<0.0001$, **= $P<0.01$, n.s.=not significant.

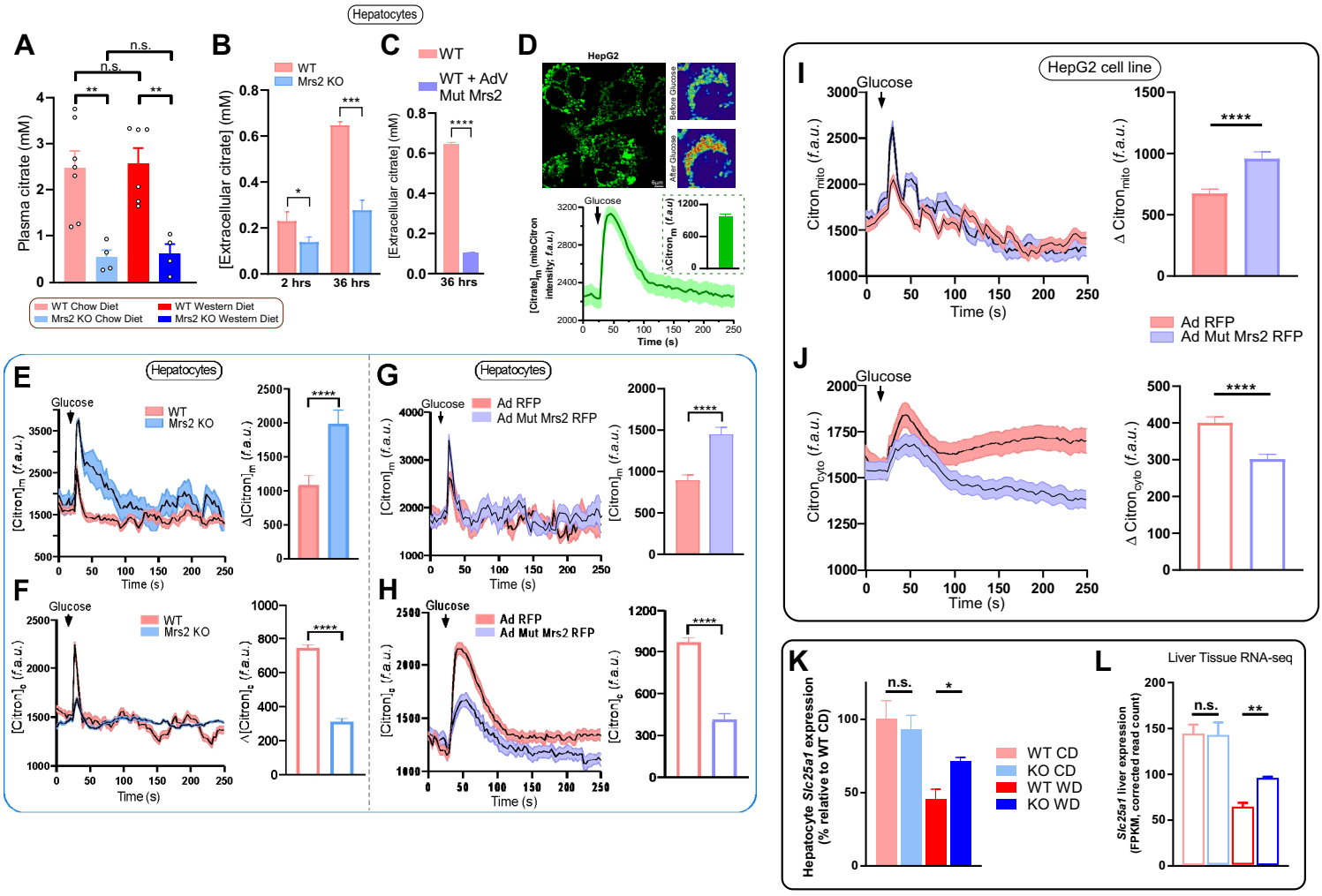
A
B
C
D
Hepatocytes
n.s.
Plasma citrate (mM)
WT Chow Diet
Mrs2 KO Chow Diet
WT Western Diet
Mrs2 KO Western Diet
[Extracellular citrate] (mM)
WT
Mrs2 KO
2 hrs
36 hrs
WT + AdV Mut Mrs2
HepG2
Before Glucose
After Glucose
Glucose
Time (s)
E
F
G
H
[Citron]m (f.a.u.)
[Citron]c (f.a.u.)
Δ[Citron]m (f.a.u.)
Δ[Citron]c (f.a.u.)
Ad RFP
Ad Mut Mrs2 RFP
I
J
HepG2 cell line
Citronmito (f.a.u.)
Δ Citronmito (f.a.u.)
Citroncyto (f.a.u.)
Δ Citroncyto (f.a.u.)
K
L
Hepatocyte Slc25a1 expression (% relative to WT CD)
WT CD
KO CD
WT WD
KO WD
Liver Tissue RNA-seq
Slc25a1 liver expression (FPKM, corrected read count)

Figure S5. Genetic deletion of Mrs2 or Reconstitution of Loss-Of-Function Mrs2 Mutant Suppress Mitochondrial Citrate Efflux. (Related to Figure 5).

A) Plasma citrate levels were measured in WT and *Mrs2*$^{-/-}$ mice fed with chow or Western diet. n = 4-7 mice/group.
B) Extracellular citrate production after 2 hours (left) and 36 hours (right) of WT and Mrs2 KO hepatocytes in culture. n=3 per time point.
C) Extracellular citrate production in isolated hepatocyte culture after 36 hours of infection with adenovirus expressing mutant Mrs2. n=3.
D) Representative image of HepG2 cells expressing mitochondria targeted citrate sensor Citron1. The pseudocolored images depict the mito-Citron dynamic fluorescence change upon glucose (17 mM) stimulation. Trace depictsmito-Citron1 fluorescence dynamics after glucose stimulation and the inset is the quantification of citrate production (amplitude;peak – pre-addition)
E) Measurement (left) and quantification (right) of mito-Citron1 dynamics in WT or *Mrs2*$^{-/-}$ hepatocytes after stimulation with 20 mM glucose. n=3.
F) Measurement (left) and quantification (right) of cytosolic-Citron1 dynamics in WT or *Mrs2*$^{-/-}$ hepatocytes after stimulation with 20 mM glucose. n=3.
G) Measurement (top) and quantification (bottom) of mito-Citron1 dynamics in WT hepatocytes infected with either Ad-RFP or Ad-mutant-Mrs2-RFP. Stimulated with 20 mM glucose. n=3.
H) Measurement (top) and quantification (bottom) of cytosolic-Citron1 dynamics in WT hepatocytes infected with either Ad-RFP or Ad-mutant-Mrs2-RFP. Stimulated with 20 mM glucose. n=3.
I) and J) Measurement (left) and quantification (right) of mito-Citron1 (I) or cyto-Citron1 (J) dynamics in HepG2 cell line infected with either Ad-RFP or Ad-mutant-Mrs2-RFP. 17 mM glucose stimulation. n=3.
K) Normalized *Slc25a1* gene expression in isolated hepatocytes from CD or WD-fed WT and *Mrs2*$^{-/-}$ mice. Data represented as % of WT CD.. n=3 per group. *=p<0.05, n.s.=not significant.
L) Differential gene expression analysis of *Slc25a1* in liver tissue (RNA-seq). Data represented as the corrected read count (FPKM). n=3 per group.
A-L) Data represented as mean ± SEM. (A, K) One-way ANOVA; **= P<0.01, *= P<0.05, n.s.=not significant. (B,C,E-K) Two-tailed Student's t-test; ****= p<0.0001, ***= p<0.001, *= p<0.05.

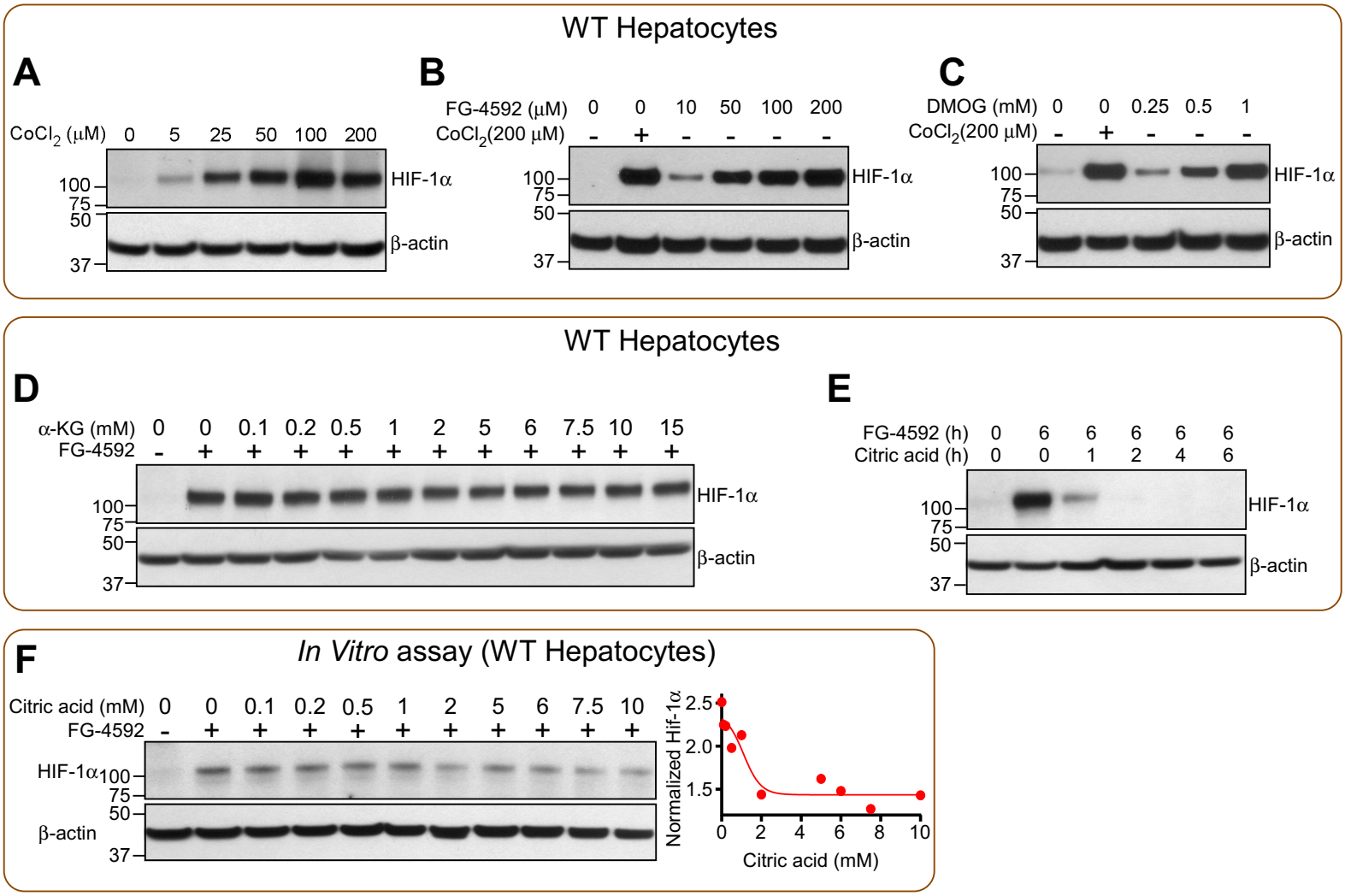
WT Hepatocytes
A
CoCl2 (μM) 0 5 25 50 100 200
100
75
50
37
HIF-1α
β-actin
B
FG-4592 (μM) 0 0 10 50 100 200
CoCl2(200 μM) - + - - - -
100
75
50
37
HIF-1α
β-actin
C
DMOG (mM) 0 0 0.25 0.5 1
CoCl2(200 μM) - + - - -
100
75
50
37
HIF-1α
β-actin
WT Hepatocytes
D
α-KG (mM) 0 0 0.1 0.2 0.5 1 2 5 6 7.5 10 15
FG-4592 - + + + + + + + + + + +
100
75
50
37
HIF-1α
β-actin
E
FG-4592 (h) 0 6 6 6 6 6
Citric acid (h) 0 0 1 2 4 6
100
75
50
37
HIF-1α
β-actin
F
In Vitro assay (WT Hepatocytes)
Citric acid (mM) 0 0 0.1 0.2 0.5 1 2 5 6 7.5 10
FG-4592 - + + + + + + + + + +
HIF-1α
β-actin
100
75
50
37
Normalized Hif-1α
2.5
2.0
1.5
0 2 4 6 8 10
Citric acid (mM)

Figure S6. Citrate Destabilizes FG-4592, $CoCl_2$ or DMOG-Induced HIF-1α Protein in Hepatocytes (Related to Figure 5).

A-F) FG-4592, $CoCl_2$ or DMOG induced HIF-1α stabilization in WT hepatocytes were treated for 6 hours and total lysates were subjected to Western blot analysis to determine HIF-1α protein abundance. n=2-3 independent hepatocyte isolations.
E) FG-4592 mediated HIF1α stabilization is destabilized by citrate in a time-dependent fashion. As indicated, citrate (10 mM) was added to FG-4592 (100 μM) hepatocytes. n=2 independent hepatocyte isolations.
F) FG-4592 treated hepatocytes were permeabilized and challenged with citrate at various concentration in vitro. Quantification of HIF1α protein abundance from the Western blot. n=2 independent experiments.

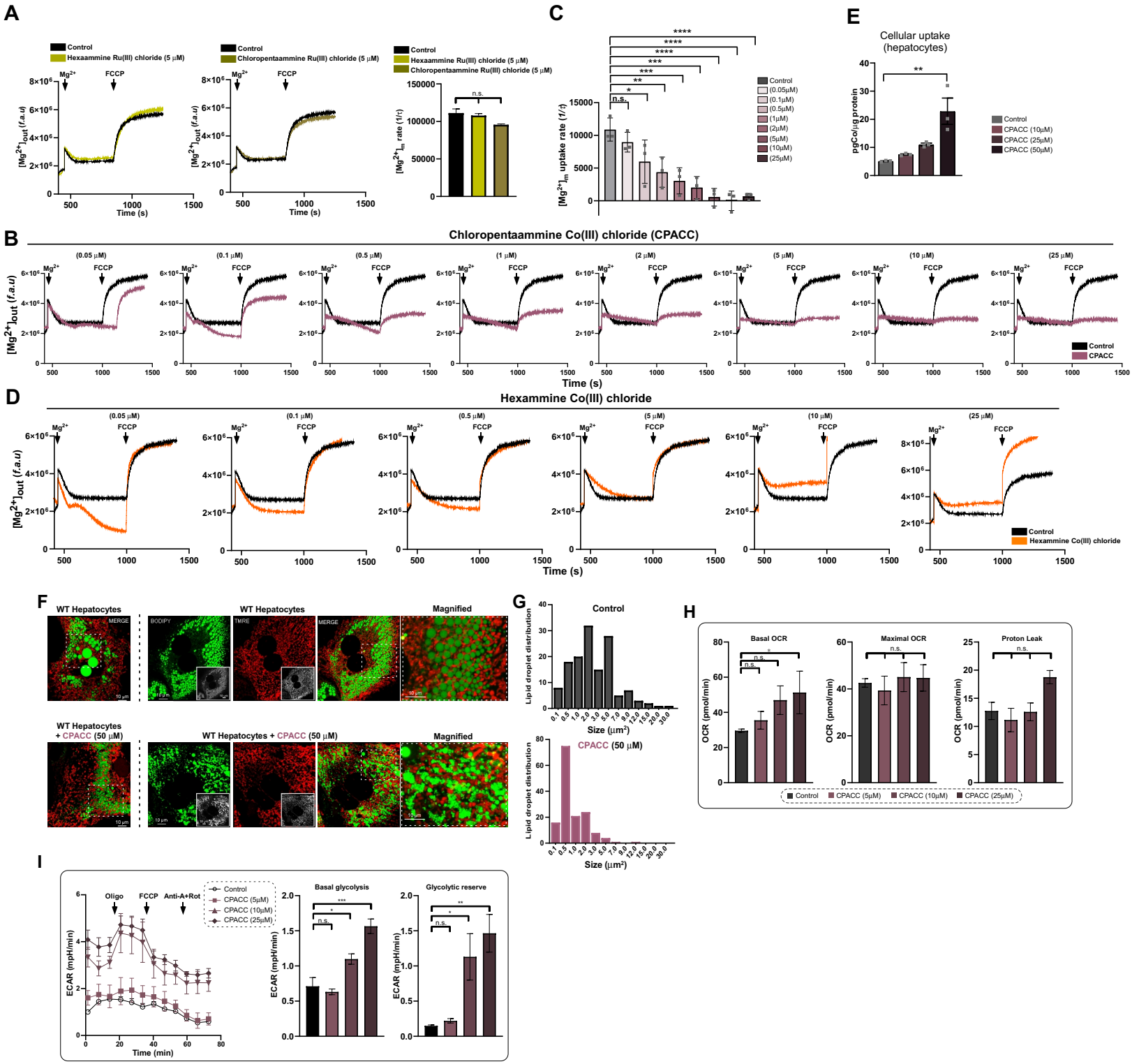
A
Control
Hexaammine Ru(III) chloride (5 μM)
Chloropentaammine Ru(III) chloride (5 μM)
Mg2+
FCCP
[Mg2+]out (f.a.u)
Time (s)
n.s.
[Mg2+]in rate (1/τ)
C
[Mg2+]in uptake rate (1/τ)
(0.05μM)
(0.1μM)
(0.5μM)
(1μM)
(2μM)
(5μM)
(10μM)
(25μM)
E
Cellular uptake
(hepatocytes)
pgCo/μg protein
CPACC (10μM)
CPACC (25μM)
CPACC (50μM)
B
Chloropentaammine Co(III) chloride (CPACC)
(0.05 μM)
(0.1 μM)
(0.5 μM)
(1 μM)
(2 μM)
(5 μM)
(10 μM)
(25 μM)
CPACC
D
Hexammine Co(III) chloride
F
WT Hepatocytes
MERGE
BODIPY
TMRE
Magnified
WT Hepatocytes + CPACC (50 μM)
G
Control
CPACC (50 μM)
Lipid droplet distribution
Size (μm²)
H
Basal OCR
Maximal OCR
Proton Leak
OCR (pmol/min)
Control
CPACC (5μM)
CPACC (10μM)
CPACC (25μM)
I
Oligo
FCCP
Anti-A+Rot
ECAR (mpH/min)
Time (min)
Basal glycolysis
Glycolytic reserve

Figure S7. The Effect of Cobalt or Ruthenium Derivatives on Mrs2-Mediated $_{m}Mg^{2+}$ Uptake and Mitochondrial Function (Related to Figures 6 and 7).

A-D) Permeabilized hepatocytes were treated with various concentrations of pretreatment. chloropentaammine Co(III) chloride, Ru (III) hexaammine chloride, chloropentaammine Ru (III) chloride, or cobalt (III) hexaammine chloride and then pulsed with 1 mM $MgCl_2$ and FCCP at the indicated time points. Representative traces show the uptake and the release of Mg^{2+} from the mitochondria (A, B, and D). Quantification of the uptake rate from Fig S7B (C). n=3-4.
E) Cellular uptake of CPACC in WT hepatocytes. Intracellular Co(III) was measured by atomic absorption spectroscopy. n=3.
F) Visualization and appearance of hepatocytes isolated from 12 months old WT mice using BODIPY-488 to label lipid droplets (left) and $\Delta\Psi_m$ indicator TMRE (middle), with or without CPACC (50μM) treatment for 48 hours. Left-most images are merged channel of images from Fig. 7A. Right-most images are merged, magnified images of images. Black and white images were generated for both TMRE and BODIPY staining (inset). Scale bar 10μM.
G) Size distribution of lipid droplets in hepatocytes following CPACC treatment (50μM). The area of droplet size was quantified from multiple cells. n=3.
H) Bar charts depict basal respiration, maximal respiration, and proton leak from Figure 7D traces. Mean ± SEM. n=3-6.
I) Traces (left) represent extracellular acidification rate (ECAR) in WT hepatocytes (12 months old mice) with varying concentrations of CPACC treatment. Inhibitors (oligomycin, FCCP, and rotenone + antimycin added at the indicated time points. Bar charts show basal glycolysis and glycolytic reserve. Mean ± SEM. n=3-5.
C, F, G-I) Data shown as mean ± SEM. ****= P<0.0001, ***= P<0.001, **= P<0.01, *= P<0.05, n.s.=not significant.